GEOPHYSICAL RESEARCH LETTERS, VOL. 37, L11802, doi:10.1029/2010GL043309, 2010

Role of Rossby wave breaking in the west Pacific teleconnection

G. Rivière[1]

Received 19 March 2010; revised 27 April 2010; accepted 28 April 2010; published 2 June 2010.

[1] The dynamical link between the west Pacific (WP) teleconnection and Rossby wave breaking (RWB) events is analyzed during winter months using ERA40 reanalysis data from 1957 to 2002. The WP pattern which is characterized by latitudinal fluctuations of the Pacific jet is closely linked to variations in the nature of RWB, similarly to the North Atlantic Oscillation. More anticyclonic (cyclonic) RWBs than usual occur in the Central Pacific during the positive (negative) WP phase when the Pacific jet is more to the north (south) than usual. Time lag daily composites show that before the occurrence of an anticyclonic RWB event, WP anomalies close to the positive phase preexist that are then reinforced during the breaking leading to an increase of the WP index even few days after the peak of the event. Cyclonic RWB events have similar but opposite effects on the WP pattern since they trigger and maintain the negative phase. Finally, a comparison with the RWB anomalies of the Pacific-North American (PNA) teleconnection is provided.
Citation: Rivière, G. (2010), Role of Rossby wave breaking in the west Pacific teleconnection, *Geophys. Res. Lett.*, *37*, L11802, doi:10.1029/2010GL043309.

1. Introduction

[2] The west Pacific (WP) teleconnection is one major mode of atmospheric variability of the Northern Hemisphere [*Barnston and Livezey*, 1987] but has been less intensively studied than the North Atlantic Oscillation (NAO) and the Pacific-North American (PNA) teleconnections which are usually found to be the two dominant patterns. Using rotated principal component analysis, the WP pattern systematically corresponds to the third or fourth empirical orthogonal function of the Northern Hemisphere on all time scales [*Feldstein*, 2000]. Similarly to the NAO, it is characterized by a north-south dipolar structure in geopotential centered at latitude 50°N (see Figure 1a) leading to meridional fluctuations of the Asian-Pacific jet.

[3] The PNA is characterized by an eastward extension/retraction of the Pacific jet and the WP and PNA jet fluctuations are thus in near quadrature [*Linkin and Nigam*, 2008].

[4] Recent studies have underlined the dynamical link that exists between synoptic Rossby wave-breaking (RWB) and teleconnections such as the NAO [*Benedict et al.*, 2004; *Rivière and Orlanski*, 2007; *Martius et al.*, 2007; *Woollings et al.*, 2008; *Strong and Magnusdottir*, 2008] or the PNA [*Orlanski*, 2005; *Martius et al.*, 2007]. The different phases of the NAO are triggered and reinforced by different kinds of RWB, the positive and the negative phases being closely related to anticyclonic (hereafter denoted as LC1 or AWB) and cyclonic (LC2 or CWB) wave-breaking events, respectively. As underlined by *Rivière* [2009], this relationship reflects a more general one between the latitudinal position of the jet and the nature of RWB. Indeed, baroclinic Rossby waves exert a positive feedback on the latitudinal fluctuations of the zonal winds; AWB (CWB) favors, and is favored by, a northward (southward) shift of the jet. The different phases of the PNA which is more characterized by pulsing of the Pacific jet rather than by its latitudinal wobbling are less clearly distinguishable in terms of the nature of RWB [*Martius et al.*, 2007]. The positive and negative phases of the PNA present respectively more and less CWB events than usual while no significant change in AWB has been detected by the previous study.

[5] Since the WP teleconnection is related to the latitudinal vacillation of the East Asian-Pacific jet, the purpose of our study is to check that its different phases can be related to variations in the nature of RWB and more precisely to document the spatial and temporal relationships between the WP pattern and RWB.

[6] The paper is organized as follows. After describing the data and the RWB detection method in section 2, the results are presented in section 3 and discussed in section 4.

2. Data and Method

[7] Monthly and daily datasets of the 40-yr European Centre for Medium-Range Weather Forecasts (ECMWF) Re-Analysis (ERA-40) at 2.5° spatial resolution for winters from December 1957 to February 2002 (DJF) are used in the present study. The wave-breaking detection method is the same as that described by *Rivière et al.* [2010] and is based on the identification of local reversals of the 200-hPa absolute-vorticity gradient.

[8] The value 1 is assigned to the event parameter $\beta_a(\lambda, \phi, t)$ ($\beta_c(\lambda, \phi, t)$) at day t at the longitude-latitude grid-point (λ, ϕ) if the algorithm detects an anticyclonic (cyclonic) overturning of the absolute-vorticity contours close to that point. The frequency distribution of AWB (CWB) is then defined as the composite of $\beta_a(\lambda, \phi, t)$ ($\beta_c(\lambda, \phi, t)$) for different days t.

[9] This composite is hereafter denoted as $\gamma_a(\lambda, \phi)$ ($\gamma_c(\lambda, \phi)$).

[10] The monthly WP and PNA indices are taken from the Climate Prediction Center (CPC) of the National Oceanic and Atmospheric Administration. The WP anomaly shown in Figure 1a is the regression of the 200-hPa geopotential on the CPC WP index. Monthly composites of the positive and negative phases of the WP (PNA) teleconnection are computed with the WP (PNA) index exceeding respectively its positive and negative standard deviation and will be denoted as WP+ (PNA+) and WP− (PNA−). A daily WP index is also constructed by projecting the daily 200-hPa low-

[1]CNRM, GAME, Météo-France, CNRS, Toulouse, France.

0094-8276/10/2010GL043309

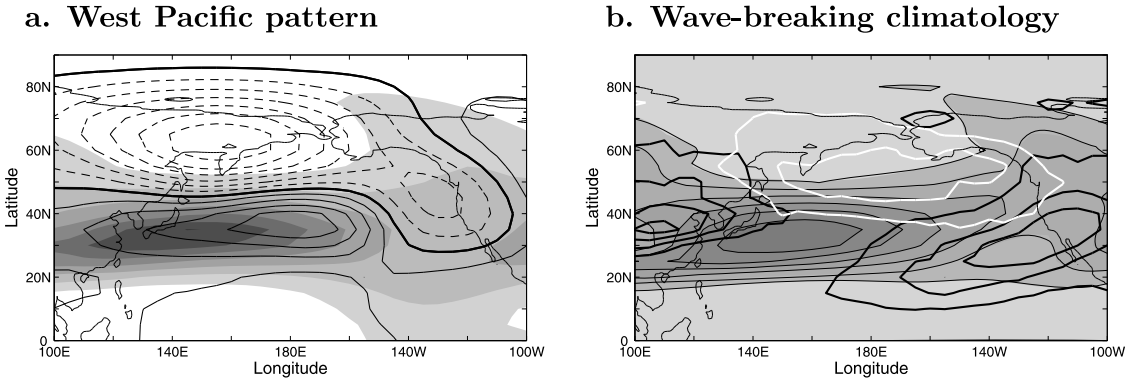

Figure 1. (a) Winter time average of the zonal wind at 200 hPa (shaded areas for values greater than 10 ms^{-1}, interval: 10 ms^{-1}) and regression of the geopotential on the monthly WP index at 200 hPa (black dashed and solid contours for negative and positive values, respectively; interval: 100 m^2s^{-2}). (b) Winter time average of the zonal wind at 500 hPa (shaded and thin black contours for values greater than 5 ms^{-1}, interval: 5 ms^{-1}) and frequency of occurrence at 200 hPa of AWB (γ_a in black contours; interval: 0.05 day^{-1}) and CWB (γ_c in white contours; interval: 0.05 day^{-1}).

frequency (periods greater than 10 days) geopotential anomalies onto the monthly WP anomaly.

3. Results

[11] CWB events occur at the entrance and in the middle of the Pacific storm-track on the north side of the jet while AWB at the end of the storm-track on the south side of the jet (Figure 1b). The pattern of high density of AWB events at longitude 100°E will not be the focus of the present study since it is not related to the storm-track eddy activity and does not vary with the WP index.

[12] Figure 2 depicts RWB statistics and jet properties for the different phases of the WP teleconnection. The jet for WP+ (Figures 2a and 2c) is characterized by a southwest-northeast orientation whereas that for WP− (Figures 2b and 2d)

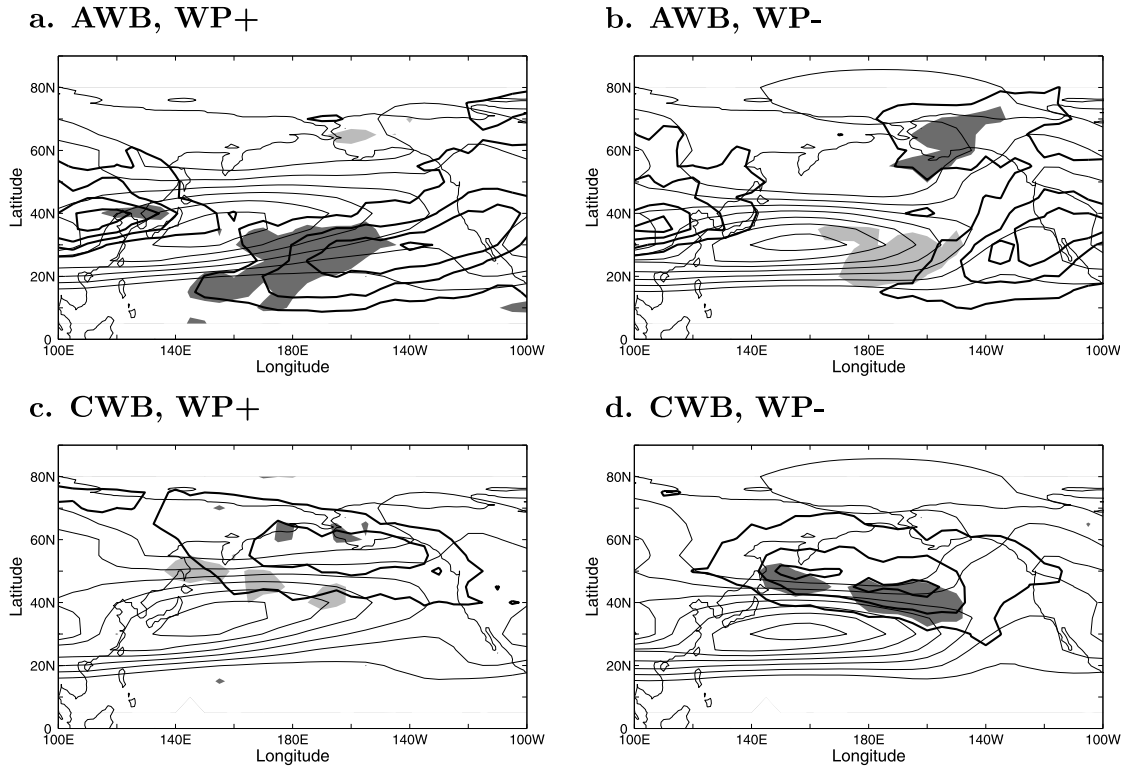

Figure 2. Monthly composites of the zonal wind at 500 hPa (thin black contours for values greater than 5 ms^{-1}, interval: 5 ms^{-1}) and the frequencies of wave-breaking occurrence at 200 hPa (thick black contours, interval 0.05 $day^{(-1)}$) for different phases of the WP teleconnection and different kinds of breaking (cyclonic and anticyclonic). Light and dark shaded areas correspond respectively to the regions where the frequencies of occurrence are significantly (98%) less and greater than their climatological mean using a t test. (a and b) Anticyclonic wave-breaking statistics γ_a when the monthly WP index exceeds one positive and negative standard deviation, respectively. (c and d) Same as Figures 2a and 2b but for cyclonic wave breaking γ_c.

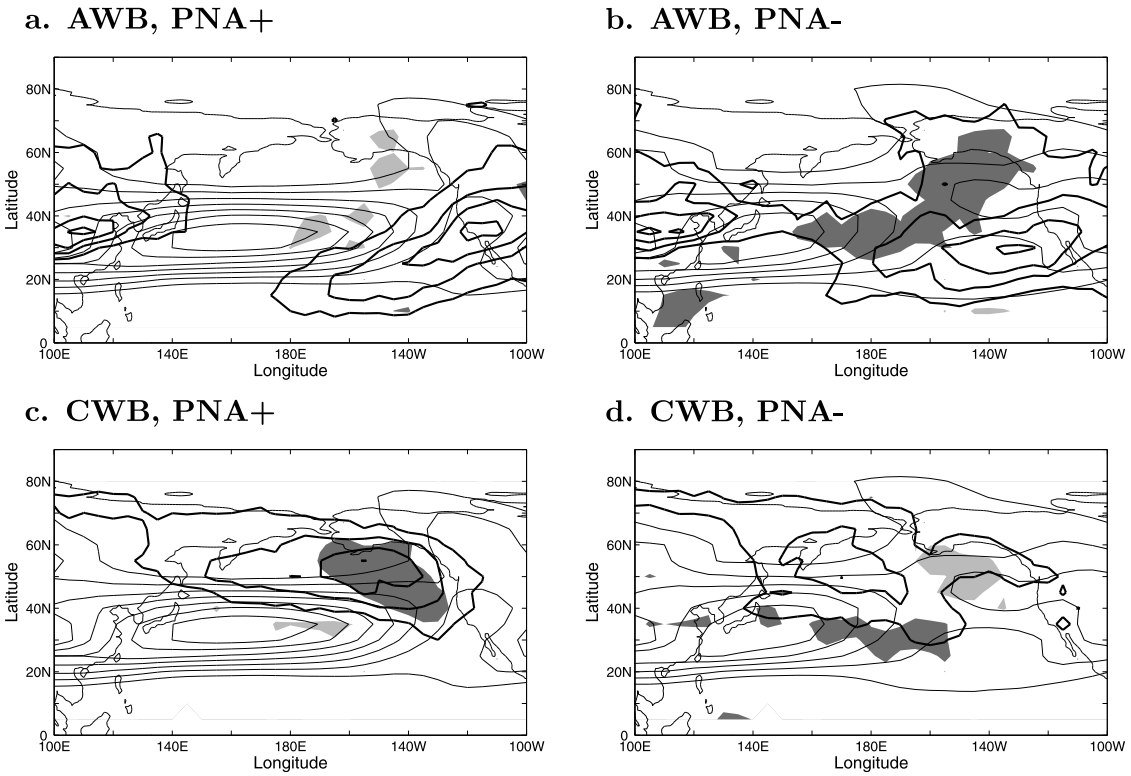

Figure 3. Same as in Figure 2 but for the PNA teleconnection.

is more zonally oriented from 140°E to 140°W. This distinction between the two extreme phases of the WP pattern is similar to the NAO case. However, the NAO latitudinal fluctuations of the Atlantic jet are stronger than the WP shifts of the Pacific jet. The major difference in AWB frequency distribution between the two WP phases appears in the area (150°E–150°W, 10°N–40°N). During WP+, AWB is significantly more frequent in that region than in the climatology while it is much less frequent during WP− (see the shaded areas in Figures 2a and 2b). This difference can be also noticed by the large area spanned by γ_a(WP+) from 150°E to North America compared to the small area covered by γ_a(WP−) from 170°W to North America (see the thick black contours in Figures 2a and 2b). Another significant difference between WP− and the climatology appears over Alaska with more AWB than usual during WP−. This maximum of γ_a cannot be directly related to the classical LC1 type of *Thorncroft et al.* [1993]. Indeed, this kind of event on the north side of the jet is often associated with the formation of an Ω-shape in the absolute-vorticity contour (not shown). In that case, our WB algorithm detects a CWB event to the west of the Ω-shape and an AWB event to the east.

[13] γ_c(WP+) (Figure 2c) and γ_c(WP−) (Figure 2d) are significantly different from the climatology. Less and more CWB events than usual in the area (140°E–150°W, 35°N–55°N) occur during WP+ and WP−, respectively. For WP+, this decrease of CWB events in that region corresponds more to a poleward shift of their frequency distribution (compare the white contours in Figure 1b to the black ones in Figure 2c). But for WP−, the increase of CWB events in the same region is linked to both a southward shift of their distribution and an overall increase of their frequency in the Pacific area (the maximum of the black contours in Figure 2d is greater than that of the white contours in Figure 1b).

[14] Since the WP and PNA are closely linked to the Pacific storm track, it is important to emphasize the differences between the two teleconnections.

[15] PNA+ corresponds to an eastward extended jet (Figures 3a and 3c) while PNA− to a retracted jet and a slight poleward shift around 140°W (Figures 3b and 3d). As expected from the difference between the WP and PNA patterns, their corresponding RWB anomalies are not located in the same regions in the Pacific. For the PNA, they are essentially centered in the Eastern Pacific from 180°E to North America (Figure 3) while those for the WP in the Western and central Pacific from 140°E to 140°W (Figure 2). γ_a(PNA+) (Figure 3a) and γ_a(PNA−) (Figure 3b) span respectively a smaller and larger area in the Eastern Pacific than in the climatology but there is only one contour difference between γ_a(PNA+) and γ_a(PNA−) in the statistically-significant regions (shaded areas). The anomalies are statistically significant but weak. For comparison, there were three contours separating γ_a(WP+) and γ_a(WP−) in the equivalent shaded areas (Figures 2a and 2b). In other words, the different phases of the WP are more distinguishable in AWB statistics than those of the PNA. However, γ_c(PNA+) (Figure 3c) and γ_c(PNA−) (Figure 3d) differ significantly to the south of Alaska and exhibit strong anomalies since they are separated by 2 to 3 contours. Therefore, more CWB events occur in the Eastern Pacific during PNA+ and much less during PNA−.

[16] Figure 4 depicts the time lag correspondences between the WP teleconnection and RWB events. Composites have been made by detecting all the AWB events occurring in the small box A = 170°W–150°W, 15°N–35°N (Figure 4e) and all the CWB events in the area B = 170°W–

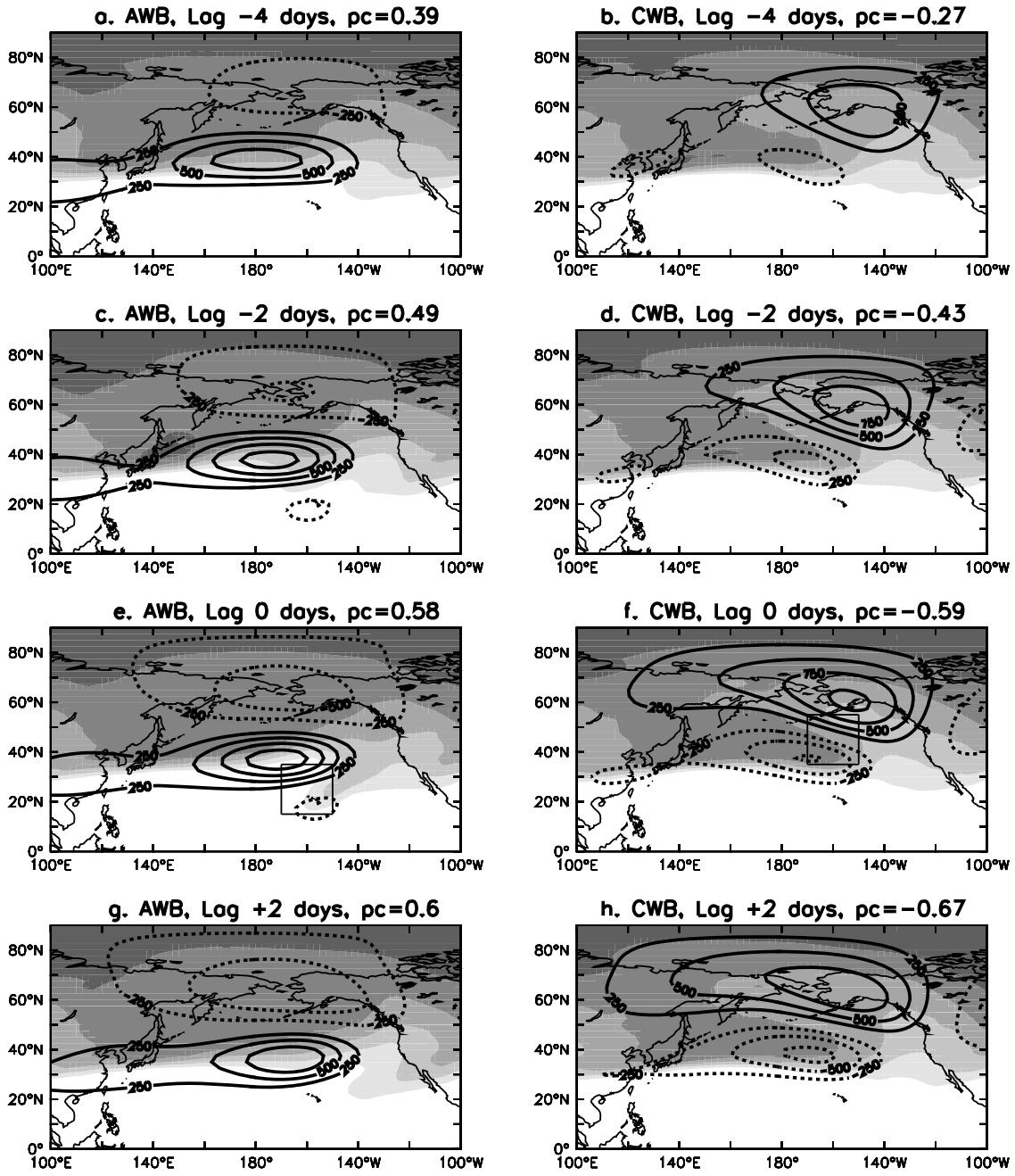

Figure 4. Daily composites of absolute vorticity (shadings; interval: 2 10^{-5} s^{-1}) and low-frequency (periods greater than 10 days) geopotential (black dashed and solid contours for negative and positive values, respectively; interval: 250 m^2s^{-2}) for (left) AWB events occurring in the area A (thin lines in Figure 4e) and (right) CWB events occurring in area B (thin lines in Figure 4f). Time lags and the WP index are indicated. See more details in the text.

150°W, 35°N–55° N (Figure 4f). These two areas have been chosen to correspond respectively to the largest differences in γ_a and γ_c between WP– and WP+ (see Figure 2) that are significantly different from the climatology.

[17] Let us denote $[\beta_a]_A(t)$ the spatial average of $\beta_a(\lambda, \phi, t)$ over the area A. An AWB event enters in the composite if $[\beta_a]_A(t)$ exceeds one and a half times its standard deviation and if $[\beta_a]_A(t) > [\beta_a]_A(t-1)$ and $[\beta_a]_A(t) > [\beta_a]_A(t+1)$, the last two conditions serving as a detection of the peak of the event.

[18] An equivalent composite has been built for CWB over the area B. The AWB and CWB composites obtained include respectively 227 and 243 days which correspond to one to two events per month for each composite.

[19] 4 days before the AWB event in area A (Figure 4a), the positive anomaly of the WP pattern is already present and the WP index equals 0.39. Then, from lag −4 to lag 0 days, there is a reinforcement of the low-frequency geopotential anomalies and an increase of the WP index. At lag 0 days, the breaking event is well visible in Figure 4e, it is characterized by a southwest-northeast tilted cyclonic anomaly in the area A that can be seen from the reversal of two absolute-vorticity contours. Between lag −4 and lag 0 days, there is an increase of the positive anomaly of the low-frequency geopotential to

the northeast of the breaking area and the appearance of a slight negative anomaly to the southwest that will then disappear at lag +2 days. The latter anomaly seems to be quite anecdotic for the WP oscillation since it is not related to the dipolar structure but should be linked to Kona lows [*Moore et al.*, 2008]. During the breaking, the amplification of the positive anomaly reinforces the WP dipolar structure as well as does the negative anomaly located farther to the north around 70° N. The intensity of the positive anomaly decreases between lag 0 and lag +2 days but the negative anomaly keeps amplifying leading to a very slight increase of the WP index at the end of the breaking event reaching 0.60 at lag +2 days.

[20] At lag −4 days, the CWB composite (Figure 4b) presents a weaker amplitude in the low-frequency geopotential anomaly than the AWB composite (Figure 4a). This suggests that the occurrence of a CWB event is less dependent on the pre-existence of WP anomalies than the AWB event. The cyclonic overturning of the absolute vorticity is already visible few days before the peak of the event but is significantly reinforced at lag 0 days in the area B. From lag −4 to lag +2 days, the dipolar structure of WP− appears more and more clearly, keeps amplifying after the breaking and the WP index reaches its minimum −0.67 at lag +2 days. The relationship between the WP dipolar structure and the breaking is clearer for the CWB event; at lag −4 days, the two poles are well localized (which is less the case for the AWB event) and form a southwest-northeast axis and during the next days, each pole extends more and more zonally and the dipolar structure gets more and more a south-north orientation. The latter properties are typical of a breaking event.

4. Summary and Discussion

[21] The WP oscillation, similarly to the NAO, is intrinsically related to fluctuations in the nature of wave breaking. The positive (negative) phase presents more (less) AWB and less (more) CWB events than usual in the Central Pacific. AWB events in this region are favored by the pre-existence of WP+, but then reinforce the pre-existing anomalies during and after the breaking. CWB events have similar but opposite effects on WP since they trigger and maintain WP−. However, their occurrence is less dependent on pre-existing anomalies of WP− and seems to be more sudden. This behavior reflects the positive eddy feedback acting on the latitudinal fluctuations of the jets discussed in *Rivière* [2009]. In the latter study, it is shown that a more northward (southward) jet favors the occurrence of AWB (CWB) that in turn tends to maintain the jet more to the north (south). Similarly, in the present case, when the jet is angled more northeastward into the Gulf of Alaska (WP+), AWB accelerates the jet northeastward and when the jet is more zonal and more to the south (WP−), CWB zonally accelerates the jet and preserves its more southward position.

[22] RWB anomalies of the PNA appear in the Eastern Pacific but present less symmetries between CWB and AWB, consistently with [*Martius et al.*, 2007] findings. PNA+ is favored by a significant increase of CWB events to the south of Alaska while PNA− by a suppression of such events. AWB anomalies are less clearly identified even though PNA− is linked to a slight increase of AWB events and an extension of the zones where they occur. The fact that the PNA phases are less well distinguishable in the nature of RWB may come from the intrinsic property of the PNA which is characterized by pulsing of the Pacific jet.

[23] By analyzing RWB statistics in climate simulations of the Last Glacial Maximum (LGM), *Rivière et al.* [2010] have shown that the NAO for the latter climate was characterized by pulsing of the Atlantic jet and its extreme phases did not differ in the type of RWBs in contrast with the present climate. The positive phase of the NAO in LGM simulations exhibits more an eastward extended jet which is linked to both an increase of AWB and CWB frequencies of occurrence to the east. In that sense, the LGM NAO is close to the PNA of the present climate.

[24] **Acknowledgment.** This work was supported by ANR contract JCJC-06-139163.

References

Barnston, A. G., and R. E. Livezey (1987), Classification, seasonality and persistence of low-frequency atmospheric circulation patterns, *Mon. Weather Rev.*, *115*, 1083–1126.

Benedict, J. J., S. Lee, and S. B. Feldstein (2004), Synoptic view of the North Atlantic Oscillation, *J. Atmos. Sci.*, *64*, 121–144.

Feldstein, S. B. (2000), The timescale, power spectra, and climate noise properties of teleconnection patterns, *J. Clim.*, *13*, 4430–4440.

Linkin, M. E., and S. Nigam (2008), The North Pacific Oscillation- west Pacific teleconnection pattern: Mature-phase structure and winter impacts, *J. Clim.*, *21*, 1979–1997.

Martius, O., C. Schwierz, and H. C. Davies (2007), Breaking waves at the tropopause in the wintertime Northern Hemisphere: Climatological analyses of the orientation and the theoretical LC1/2 classification, *J. Atmos. Sci.*, *64*, 2576–2592.

Moore, R. W., O. Martius, and H. C. Davies (2008), Downstream development and Kona low genesis, *Geophys. Res. Lett.*, *35*, L20814, doi:10.1029/2008GL035502.

Orlanski, I. (2005), A new look at the Pacific storm track variability: Sensitivity to tropical SSTs and to upstream seeding, *J. Atmos. Sci.*, *62*, 1367–1390.

Rivière, G. (2009), Effect of latitudinal variations in low-level baroclinicity on eddy life cycles and upper-tropospheric wave-breaking processes, *J. Atmos. Sci.*, *66*, 1569–1592.

Rivière, G., and I. Orlanski (2007), Characteristics of the Atlantic Storm-track eddy activity and its relation with the North Atlantic Oscillation, *J. Atmos. Sci.*, *64*, 241–266.

Rivière, G., A. Laîné, G. Lapeyre, D. Salas-Mélia, and M. Kageyama (2010), Links between Rossby wave breaking and the North Atlantic Oscillation - Arctic Oscillation in present-day and Last Glacial Maximum climate simulations, *J. Clim.*, *23*, 2987–3008, doi:10.1175/2010JCLI3372.1.

Strong, C., and G. Manusdottir (2008), Tropospheric Rossby wave breaking and the NAO/NAM, *J. Atmos. Sci.*, *65*, 2861–2876.

Thorncroft, C. D., B. J. Hoskins, and M. McIntyre (1993), Two paradigms of baroclinic-wave life-cycle behaviour, *Q. J. R. Meteorol. Soc.*, *119*, 17–55.

Woollings, T., B. Hoskins, M. Blackburn, and P. Berrisford (2008), A new Rossby wave-breaking interpretation of the North Atlantic Oscillation, *J. Atmos. Sci.*, *65*, 609–626.

G. Rivière, Météo France, CNRM, GMAP, RECYF, 42 ave. G. Coriolis, F-31057 Toulouse, CEDEX 1, France. (gwendal.riviere@meteo.fr)